Phys. Status Solidi B **248**, No. 5, 1264–1269 (2011) / **DOI** 10.1002/pssb.201046437

physica status solidi b
www.pss-b.com
basic solid state physics

Vortex shells in square arrays of pinning sites

Hakan Yetis*

Department of Physics, Abant Izzet Baysal University, 14280 Bolu, Turkey

Received 11 August 2010, revised 25 September 2010, accepted 8 October 2010
Published online 9 November 2010

Keywords molecular dynamics methods, superconductors, vortices

* e-mail yetis_h@ibu.edu.tr, Phone: +90 374 2541000, Fax: +90 374 2534642

We investigate the vortex states interacting with a square array of pinning sites in a superconducting sample by using a molecular dynamics approach. An improved potential is used to model the interaction between the vortices and the pinning sites. We found several shell-type structures depending on the numbers of the vortices and pinning sites. We show that the vorticity increases with increasing of magnetic field and (meta)stable vortex shells occur due to the changes in the vorticity. We deduce that the large pinning sizes are essential to obtain higher order vortex shells. Our results are compared with those obtained from the numerical and experimental studies.

1 Introduction The flux-pinning properties of type-II superconductors can be improved by using the lithographic techniques which allow the fabrication of antidots, acting as strong pinning centers, under suitable conditions [1–3]. Results of the experimental studies performed on superconducting systems with well-arranged artificial square or triangular periodic pinning arrays indicate that the vortices can be trapped both at individual pinning sites and also at the interstitial regions between them [4–6]. Analysis of the systems which contain columnar defects (CDs) revealed the existence of multi-quanta vortices at CDs [7, 8]. Also, a series of multivortex states for large pinning radius was found by experimental [9] and numerical works [10, 11].

Earlier studies performed on charged classical particles in small [12] and mesoscopic [13] parabolic potentials disclosed the shell-type configurations. However, the existence of similar formations for the vortices has not been addressed before. The recent studies have focused on the mesoscopic superconducting systems [14–17] and found different regimes of vortex matter such as (i) the discrete vortex or multivortex state which is singly quantized vortices with vorticity L, (ii) giant vortex state for the same L but a single core. In general, the triangular Abrikosov vortex lattice is energetically favorable in the absence of pinning effects for type-II superconductors. However, recent developments have showed that the vortices can display different configurations, when they are confined in blind holes [9], pillars [18] or mesoscopic superconducting disks with radii $R > \lambda$. In mesoscopic superconducting disks or squares, the vortices form concentric vortex shells or giant vortex states in a confined geometry where the lattice order is governed by the boundary of the pinning. The common question is here which configuration is energetically favorable for the vortex states depending on the external parameters. The free energy calculations of the vortex configurations as a function of the magnetic field show that different distribution of the vortices are possible for a fixed vorticity [19]. Thus, the developments in artificially engineered pinning structures brought a new physical insight in which the multivortex or giant vortex states could be formed at the pinning sites whose radius are much larger than the coherence length (ξ).

In the previous study [11], the collective multivortex states inside the individual pinning sites as a function of pinning radius of $r_p < \lambda$ were reported. In this study, we have investigated the formation of vortex shells inside the pinning sites with increasing the number of vortices N_v and the pinning sites N_p. Our model is most relevant to thin-film superconductors where the vortices can be approximated as 2D classical objects. We study the relaxation of initially randomly distributed vortices to the stable vortex configuration in the presence of periodic arrays of pinning sites with a radius comparable to λ. We have found that it is possible to obtain vortex shells with the same vorticity but different configurations with increasing magnetic field. We did not discuss directly the stability of the vortex states but our findings are compared with those found for the cases of blind

holes [9], pillars [18], and mesoscopic superconducting disks [19]. The outline of the paper is as follows: in Section 2, we give an overview of the model and simulation technique and its parameters. The main results of the study are discussed in Section 3. The paper concludes with a brief summary of the main findings in Section 4.

2 Model The vortices are modeled as interacting classical point particles [20] in 2D and the central axis of vortices is parallel to the applied magnetic field. The overdamped equation of motion for the ith vortex is:

$$\eta \frac{\mathrm{d}\mathbf{r}_i}{\mathrm{d}t} = \mathbf{F}_{\mathrm{vv}}(\mathbf{r}_i) + \mathbf{F}_{\mathrm{vp}}(\mathbf{r}_i). \tag{1}$$

Here, $\mathbf{r}_i$ is the position of the ith vortex and η is the viscous drag coefficient. The repulsive vortex–vortex interaction force is given by:

$$\mathbf{F}_{\mathrm{vv}}(\mathbf{r}_i) = f_{\mathrm{v}} \sum_{k(\neq i)}^{N_{\mathrm{v}}} K_1\left(\frac{|\mathbf{r}_i - \mathbf{r}_k|}{\lambda}\right) \frac{\mathbf{r}_i - \mathbf{r}_k}{|\mathbf{r}_i - \mathbf{r}_k|}, \tag{2}$$

where $f_{\mathrm{v}} = \Phi_0^2/8\pi^2\lambda^3$, Φ_0 is the magnetic flux quantum, N_{v} is the number of vortices, and $K_1(r/\lambda)$ is a modified Bessel function of the second kind. Here, $|\mathbf{r}_i - \mathbf{r}_k|$ is the distance between the vortices i and k. We assume that the cutoff distance is 6λ for the vortex–vortex interactions [11]. The attractive force between a vortex and a pinning center is simulated with a Nordborg–Vinokur [21] type interaction as:

$$\mathbf{F}_{\mathrm{vp}}(\mathbf{r}_i) = -f_{\mathrm{p}} \sum_{m=1}^{N_{\mathrm{p}}} \frac{K_1(|\mathbf{r}_i - \mathbf{r}_m|/\lambda)}{K_0(r_{\mathrm{p}}/\lambda)} \times \left(\frac{K_0(|\mathbf{r}_i - \mathbf{r}_m|/\lambda) + n_m K_0(r_{\mathrm{p}}/\lambda)}{r_{\mathrm{p}} K_1(r_{\mathrm{p}}/\lambda) + (r_{\mathrm{p}}^2/2) K_0(r_{\mathrm{p}}/\lambda)}\right) \hat{\mathbf{r}}_{im}, \tag{3}$$

where $\hat{\mathbf{r}}_{im} = (\mathbf{r}_i - \mathbf{r}_m)/|\mathbf{r}_i - \mathbf{r}_m|$, $\mathbf{r}_m$ is the location of the mth pinning site, r_{p} is the pinning radius, f_{p} is the pinning strength, n_m is the number of vortices trapped inside the mth pinning site, and N_{p} is total number of the pinning sites. All forces, in our simulation, are measured in units of f_{v} and all lengths in units of λ. The time is measured in units of $t_0 = \eta\lambda/f_{\mathrm{v}}$ and the time step is $\Delta t = 0.01$. In the present simulations, the sample has a size of $10\lambda \times 10\lambda$. The pinning sites are placed as 4×4, 5×5, and 6×6 square arrays with $N_{\mathrm{p}} = 16$, 25, and 36, respectively, and the magnetic induction B varies from 0.25 to 1 T. With these parameters and forces, we perform a molecular dynamics simulation to solve Eq. (1) by using a simple Euler method with periodic boundary conditions in the $x - y$ plane for the vortices and the pinning sites. We started from a state in which the vortices were distributed randomly, then relaxed this state according to the forces in Eqs. (2) and (3). Simulations were run for 10^5 steps to ensure the stability of the final configurations for each of the results presented in the Section 3.

3 Results and discussion We report the multivortex states for three different numbers of the square arrays of the pinning sites $N_{\mathrm{p}} = 16$, 25, and 36 as a function of the number of vortices N_{v} from 205 to 821 for a fixed pinning radius $r_{\mathrm{p}} = 0.5\lambda$ and the pinning strength $f_{\mathrm{p}} = 0.5 f_{\mathrm{v}}$. We find a series of discrete vortex states characterized by the vorticity L. The main results of these calculations are presented in Fig. 1a–d for 4×4 square arrays with $N_{\mathrm{p}} = 16$. For the lowest of $N_{\mathrm{v}} = 205$ (Fig. 1a), we have found that each pinning site contains seven vortices ($L = 7$) which produce a stable polygonal state. Some of the remaining vortices are caged between the pinning sites and occupy the interstitial regions. These interstitial vortices are forced to form dimers and their orientational orderings are governed by neighboring four pinning sites. For increased number of vortices ($N_{\mathrm{v}} = 410$), all pinning sites contain two-shell structures, that is, vortices tend to form polygons and the additional vortex appears in the center as shown in Fig. 1b. Here, it is observed that three different vorticities occur as $L = 10$ (1, 9), $L = 11$ (1, 10), $L = 12$ (1, 11) inside the pinning sites. The states (1, 9) and (1, 10) are predictable stable states, but they were not seen in SEM images of the mesoscopic superconducting disks in the limits of $1 \leq L \leq 11$ [15]. However, all these states (1, 9), (1, 10), and (1, 11) are the ground states, when they are compared with those found from the free energy calculations of the vortex configurations within the framework of nonlinear Ginzburg–Landau theory [19]. We also obtained that the vorticity L increases from 7 to approximately 12 with increasing the number of vortices from 205 to 410. At this N_{v} value, the vorticity $L = 11$ looks as the most probable configuration and the state (1, 10) can be accepted as a ground state of the vortices. The vortex configurations with dimer or trimer states at the inner shells are shown in Fig. 1c and d for $N_{\mathrm{v}} = 615$ and 821. Three different two-shell structures are composed of one, two, or three vortices at the centers (inner shells) with encircling polygons (outer shells) along the periphery of the pinning sites. For $N_{\mathrm{v}} = 615$, the vorticity increases to values of $L = 14$ (1, 13), (2, 12), $L = 15$ (1, 14), (2, 13), $L = 16$ (2, 14). For $L = 14$ and 15, we obtained vortex shells with the same vorticity but different configurations inside the pinning sites. The stability of vortex configurations are in good agreement with experimental and numerical studies of mesoscopic superconducting disks for $L \leq 14$ [9, 15, 19, 22]. For highest of N_{v}, the concentration of the inner shells reaches almost three vortices, forming trimer states at the center of the pinning sites, as shown in Fig. 1d. The states (2, 15), (3, 14) for $L = 17$, (3, 15) and (3, 16) for $L = 18$ and 19 can be accepted as the metastable states of the vortex system.

In Table 1, we summarize our results mentioned above as functions of number of vortices N_{v} and number of the pinning sites N_{p}. From left to right across the Table 1, we present the L values for different number of the pinning sites for a fixed value of N_{v}. The first noticeable findings are the diminution of L and formation of different meta(stable) vortex configurations with increasing N_{p}. For the lowest value of $N_{\mathrm{v}} = 205$, the ground state configuration (0, 7) of the vortices

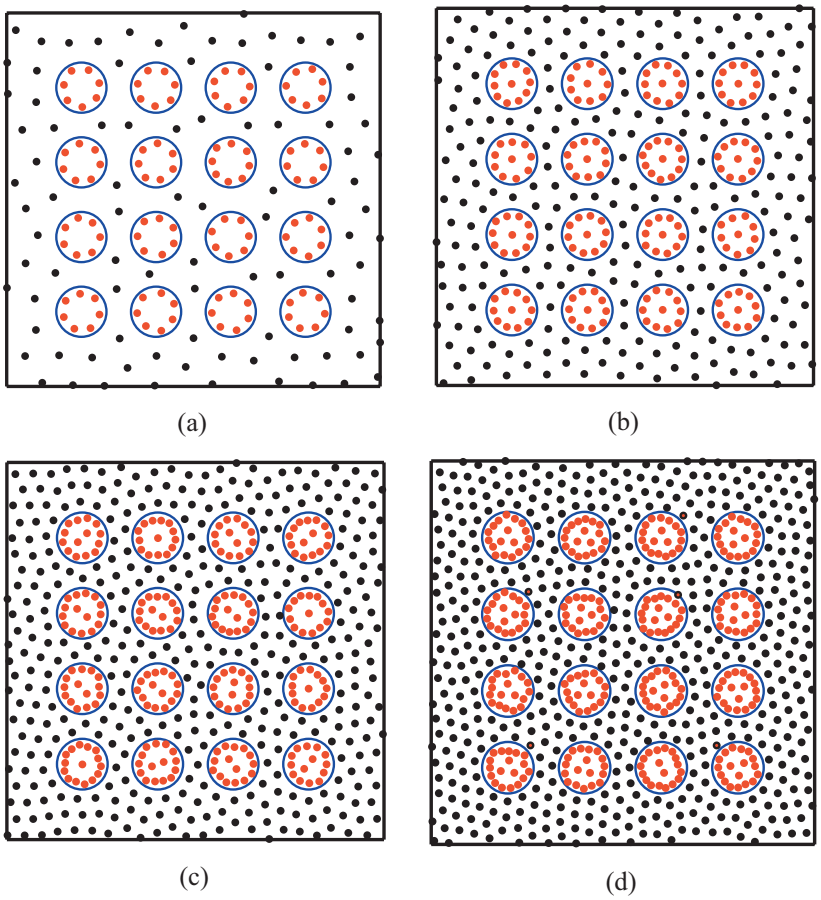

Figure 1 (online color at: www.pss-b.com) Formation of two-shell vortex configurations as a function of N_v at $f_p = 0.5f_v$ and $r_p = 0.5\lambda$: (a) $N_v = 205$, (b) $N_v = 410$, (c) $N_v = 615$, and (d) $N_v = 821$. The blue hollow circles represent the pinning sites and solid dots show the point-like vortices.

changes dramatically and turns into four different vortex states such as (trimer, square, pentagon, and hexagon) for $N_p = 36$. A similar case can be also seen for $N_v = 410$. When N_p is increased from 16 to 36, both polygonal and two-shell structures with the same vorticity but different configurations appear. The states (0, 8), (0, 9), and (0, 10) are metastable and (1, 7), (1, 8), and (1, 9) are stable states of the vortex system [19]. We suggest that formation of the different vortex states with increasing of N_p for a fixed sample size is resulted from decreasing of inter-pinning distance. A reduction of interstitial regions causes the pinning forces to overlap and the vortices are more exposed to collective attraction of the pinning sites. At this point, we have to recall the importance of the pinning force $\mathbf{F}_{vp}$ in our simulation, taking into account the number of vortices (n_m) inside the pinning sites because an empty pinning site always attracts the incoming vortices. When a first vortex enters, it interacts repulsively with the external vortices, and a potential barrier, preventing further penetrations of the other vortices, is set. In such a case, some of the pinning sites can trap more vortices compared to the others. We also observed that reducing of inter-pinning distance causes some caging effects on interstitial vortices. The vortices are forced to form single, dimer, or trimer states as a function of the N_v. For instance, at low values of the number of vortices (i.e., $N_v = 205$), no vortices are allowed at the interstitial region with increasing the number of pinning sites. At highest values of $N_v = 821$ and $N_p = 36$, the vortices form mostly trimer, also dimer and square states between the enclosing pinning arrays. This confining potential for the interstitial vortices in a small medium results from strong repulsive interactions of the pinning sites with their internal vortices. In the presence of strong confinement effects, vortices can also form a giant vortex state at the interstitial regions [23].

The results presented in Table 1 show that some metastable vortex configurations become dominant with increasing of the vorticity. Three different vortex configurations such as (1, 15), (2, 14), (3, 15) are the metastable states, when $N_v = 821$ and $N_p = 36$. These results show that L approaches to a certain number inside the pinning sites and the stable vortex states are reduced to metastable ones with increasing of N_v. For all numbers of N_p, while the vortices are displaying stable configurations for $N_v = 205$, two-shell structures with the same L, but different configurations occur for the highest of $N_v = 821$. We know from the free energy calculations, a new vortex shell must be formed with increasing the vorticity. However, we observe that further increasing of applied magnetic field inside the sample does not contribute to formation of the higher order vortex shells and reduces the stability of the vortex state. Even, high vortex

Table 1 The number of vortices in the shells obtained for $N_v = 205$, 410, 615, and 821 and $N_p = 16$, 25, and 36 at $r_p = 0.5\lambda$.

N_v	$N_p = 16$			$N_p = 25$			$N_p = 36$		
	L	(S_1, S_2)	NoS	L	(S_1, S_2)	NoS	L	(S_1, S_2)	NoS
205	7	(0, 7)	**16**	5	pentagon	1	3	trimer	1
				6	(0, 6)	**20**	4	square	10
				7	(0, 7)	4	5	pentagon	**16**
							6	(0, 6)	9
410	10	(1, 9)	3	9	(1, 8)	7	8	(0, 8)	1
	11	(1, 10)	**12**	10	(1, 9)	**14**		(1, 7)	1
	12	(1, 11)	1	11	(1, 10)	4	9	(0, 9)	6
								(1, 8)	**17**
							10	(0, 10)	2
								(1, 9)	9
615	14	(1, 13)	3	13	(1, 12)	8	12	(1, 11)	11
		(2, 12)	2		(2, 11)	2	13	(1, 12)	**20**
	15	(1, 14)	1	14	(2, 12)	**15**		(2, 11)	5
		(2, 13)	**9**						
	16	(2, 14)	1						
821	18	(2, 16)	1	16	(2, 14)	5	15	(2, 13)	**16**
		(3, 15)	**13**		(3, 13)	2	16	(1, 15)	1
	19	(3, 16)	2	17	(2, 15)	5		(2, 14)	14
					(3, 14)	**13**		(3, 13)	5

L represents the vorticity inside the pinning sites. Shell structures (S_1, S_2) are arranged from inner to outer shells. NoS is the number of states and bold numbers represent the number of the most probable states.

density has negative influence on *regular outer shells* and causes deformations on their shapes as seen in Fig. 1d. As a result, increasing the vortex density causes the formation of metastable vortex states (such as (2, 15), (3, 14), (3, 15), (3, 16)) inside the pinning sites. Namely, the interaction between vortices become more important, leading to the formation of high populated outer shells with just dimer or trimer states in the center. At this point, it is meaningful to mention about the saturation of the pinning sites. Such a case can be thought as a balance state for the interactions between the interstitial vortices and pinning sites together with their vortices. The attractive pinning sites can turn into the repulsive barriers, when they are fully occupied by the vortices. In such a case, a pinning site opposes the penetration of an extra vortex even at high vortex densities, because the vortices repel each other with greater forces, if they are brought much closer to each other. The concentration of the vortices near the edge of the pinning sites is an indication of the existence of these strong repulsive interactions. In order to determine whether a saturation occurs or not, we calculate the ratio of the number of captured vortices to the number of total vortices, called as:

$$\alpha = \frac{\text{Number of Captured Vortices(NCV)}}{\text{Number of Total Vortices(NTV)}}. \quad (4)$$

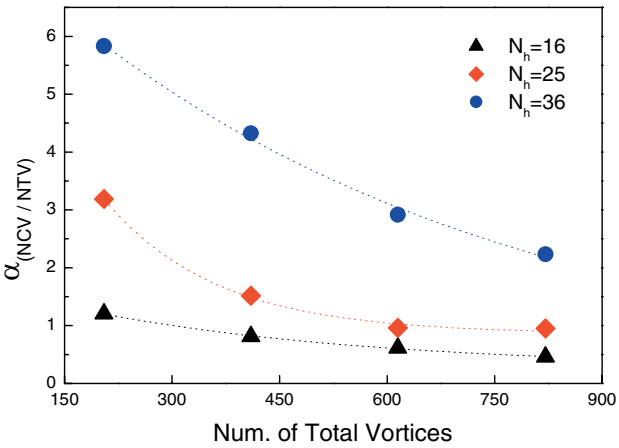

Figure 2 (online color at: www.pss-b.com) The change of α ratio as a function of total number of vortices N_v. NTV and NCV are the number of total and captured vortices, respectively.

Figure 2 shows the variation of α with respect to the number of vortices N_v for a fixed pinning strength $f_p = 0.5f_v$ and radius $r_p = 0.5\lambda$. We have found that the α number decreases exponentially with increasing the applied magnetic field, namely N_v. The decay of the α proves that the number of vortices which are allowed into the pinning sites gradually decreases and a saturation occurs although the increasing of the number of vortices. Thus, we suggest that the large pinning sizes are essential to obtain higher order vortex shells because increasing the vorticity results in the formation of metastable vortex states at small confined geometries for high values of $N_v = 615$ and 821.

Recent experiments have shown that the vortices form circular configurations inside the pinning sites at high vorticities [15, 16] even they form concentric vortex shells in the mesoscopic superconducting disks with further increasing of the vorticity [17]. Figure 3 shows numerical examples of the higher order vortex shells inside the pinning sites with radius of $r_p = 0.8\lambda$ for the number vortices of $N_v = 821$ and 1182. The sample size $12\lambda \times 12\lambda$ was also studied to show the effect of inter-pinning distance on the vortex configurations (see Fig. 3b). Three-shell structures appear with increasing the radius of pinning sites from 0.5λ to 0.8λ. Figure 3a presents vortex shells, that is, a single vortex forms the first shell (S_1), the second shell (S_2) contains pentagon or hexagon configurations of the vortices. The remaining vortices produce the outer shell (S_3) along the periphery of the pinning sites. With increasing the sample size to $12\lambda \times 12\lambda$, we also observed more concentric three-shell configurations inside the pinning sites. We deduce that strong repulsive interactions of the vortices inside the pinning sites prevent the formation of higher order vortex shells. These interactions are getting stronger with decreasing pinning radius r_p. We note that a gradual increasing of the vorticity does not mean to the formation of higher order vortex shells but increasing pinning radius is essential. The formation of vortex shells obey the filling rule as similar to

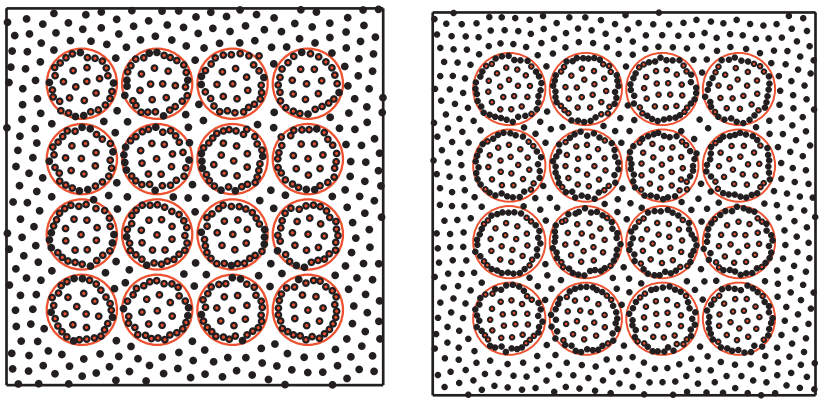

(a) (b)

Figure 3 (online color at: www.pss-b.com) Three-shell vortex structures obtained for (a) the sample size $10\lambda \times 10\lambda$ with $N_v = 821$ at $r_p = 0.8\lambda$, (b) the sample size $12\lambda \times 12\lambda$ with $N_v = 1182$ at $r_p = 0.8\lambda$.

that of the theoretical study of Misko et al. [17], and first the outer S_3 and than the second shell S_2 and finally the inner shell S_1 is formed by vortices. The vortices can also form individual giant vortex states [23] for certain parameters. For instance, at high magnetic fields, a smooth transition from vortex shell state to a giant vortex state occurs depending on the pinning radius in the mesoscopic superconducting disks [23, 24]. However, in the present work, such a giant vortex state cannot be described within our classical particle approach and Ginzburg–Landau theory is needed for that [25]. On the other hand, in our simulations, we studied vortex shells for a collective system with many vortices and pinning sites. Thus, we take into account the effects of external forces (such as magnetic pressure, neighboring pinning effects, etc.) on the evolution of the vortex states. This consideration may benefit to understand the formation of meta(stable) states in real superconducting systems.

4 Conclusion The multivortex states and vortex shells at the periodic pinning sites were studied numerically as functions of the number of the vortices N_v and the number of pinning sites N_p in a 2D superconducting sample. We observed that the vorticity at a single pinning site increases with increasing N_v and this allows the formation of the multiple vortex states and vortex shells inside the pinning sites. In addition, we obtained some vortex shells with the same vorticity but different configurations with increasing the number of the vortices. Such a case exhibits the existence of the metastable vortex states. In earlier numerical studies, the flux-pinning term was generally modeled as an attractive parabolic potential well [10] to confine the vortices inside the pinning sites. In this work, the interaction potential energy [21] is considered as the pinning energy because it takes into account the number of vortices inside the pinning sites. This consideration results in the formation of several composite meta(stable) vortex states inside the pinning sites. We also showed some missing stable vortex states contrary to experimental studies and compared our results with those obtained from the free energy calculation of the ground vortex states. The findings are in good agreement with the results of Bitter decoration experiments which give the visualization of vortex distributions. In our study the vortex configurations are compared with those found for the cases of blind holes [9, 26], pillars [18], and mesoscopic disk arrays [23, 24] because the vortex configuration within an anti-dot [27] is not relevant since we model vortices as classical particles, but the total amount of vortices can be detected. The *reasons* for stability of the vortex configurations are not considered here but the formation of vortex shells is reflected in detail with our new approach to pinning potential.

References

[1] R. Wördenweber, P. Dymashevski, and V. R. Misko, Phys. Rev. B **69**, 184504 (2004).
[2] V. Silhanek, S. Raedts, M. J. Van Bael, and V. V. Moshchalkov, Phys. Rev. B **70**, 054515 (2004).
[3] J. Van de Vondel, C. C. de Souza Silva, B. Y. Zhu, M. Morelle, and V. V. Moshchalkov, Phys. Rev. Lett. **94**, 057003 (2005).
[4] K. Harada, O. Kamimura, H. Kasai, T. Matsuda, and A. Tonomura, Science **274**, 1167 (1996).
[5] T. Matsuda, K. Harada, H. Kasai, O. Kamimura, and A. Tonomura, Science **271**, 1393 (1996).
[6] V. Metlushko, U. Welp, G. W. Crabtree, R. Osgood, S. D. Bader, L. E. DeLong, Z. Zhang, S. R. J. Brueck, B. Ilic, K. Chung, and P. J. Hesketh, Phys. Rev. B **60**, R12585 (1999).
[7] I. Buzdin, Phys. Rev. B **47**, 11416 (1993).
[8] G. M. Braverman, S. A. Gresedeskul, and Y. Avishai, Phys. Rev. B **57**, 13899 (1998).
[9] A. Bezryadin, Y. N. Ovchinnikov, and B. Pannetier, Phys. Rev. B **53**, 8553 (1996).
[10] C. Reichhardt and N. G. Jensen, Phys. Rev. Lett. **85**, 2372 (2000).
[11] H. Yetis, Phys. C **470**, 15 (2010).
[12] Y. E. Lozovik and L. M. Pomirchy, Phys. Status Solidi B **161**, K11 (1990).
[13] V. M. Bedanov and F. M. Peeters, Phys. Rev. B **49**, 2667 (1994).
[14] V. A. Schweigert, F. M. Peeters, and P. S. Deo, Phys. Rev. Lett. **81**, 2783 (1998).

[15] V. Grigorieva, W. Escoffier, J. Richardson, L. Y. Vinnikov, S. Dubonos, and V. Oboznov, Phys. Rev. Lett. **96**, 077005 (2006).
[16] V. R. Misko, B. Xu, and F. M. Peeters, Physica C **468**, 726 (2008).
[17] V. R. Misko, H. J. Zhao, F. M. Peeters, V. Oboznov, S. V. Dubonos, and I. V. Grigorieva, Supercond. Sci. Technol. **22**, 034001 (2009).
[18] G. R. Berdiyorov, V. R. Misko, M. V. Milosevic, W. Escoffer, I. V. Grigorieva, and F. M. Peeters, Phys. Rev. B **77**, 024526 (2008).
[19] B. J. Baelus, L. R. E. Cabral, and F. M. Peeters, Phys. Rev. B **69**, 064506 (2004).
[20] L. R. E. Cabral, B. J. Baelus, and F. M. Peeters, Phys. Rev. B **70**, 144523 (2004).
[21] H. Nordborg and V. M. Vinokur, Phys. Rev. B **62**, 12408 (2000).
[22] L. J. Campbell and R. M. Ziff, Phys. Rev. B **20**, 1886 (1979).
[23] G. R. Berdiyorov, M. V. Milosevic, and F. M. Peeters, Phys. Rev. B **74**, 174512 (2006).
[24] A. Kanda, B. J. Baelus, F. M. Peeters, K. Kadowaki, and Y. Ootuka, Phys. Rev. Lett. **93**, 257002 (2004).
[25] V. A. Schweigert and F. M. Peeters, Phys. Rev. B **57**, 13817 (1998).
[26] G. R. Berdiyorov, M. V. Milosevic, and F. M. Peeters, New J. Phys. **11**, 013025 (2009).
[27] G. R. Berdiyorov, M. V. Milosevic, and F. M. Peeters, Phys. Rev. Lett. **96**, 207001 (2006).